

# Reaction pathways for oxygen evolution promoted by cobalt catalyst

## Supporting Information

Giuseppe Mattioli,<sup>\*,†</sup> Paolo Giannozzi,<sup>‡,¶</sup> Aldo Amore Bonapasta,<sup>†</sup> and Leonardo  
Guidoni<sup>\*,§</sup>

*Istituto di Struttura della Materia del CNR, v. Salaria Km 29,300 - C.P. 10 I-00015 -  
Monterotondo Stazione (RM) Italy, Department of Chemistry, Physics, and Environment,  
University of Udine, via delle Scienze 208, I-33100 Udine, Italy, DEMOCRITOS CNR-IOM  
National Simulation Center, I-34014 Trieste, Italy, and Dipartimento di Scienze Fisiche e  
Chimiche, Università degli Studi de L'Aquila, Via Vetoio 2, Coppito, I-67100 L'Aquila, Italy*

E-mail: giuseppe.mattioli@ism.cnr.it; leonardo.guidoni@univaq.it

## Contents

<b>1</b>	<b>Assessment of Theoretical Methods</b>	<b>2</b>
1.1	LiCoO <sub>2</sub> Properties . . . . .	4
1.2	[Co(II)H <sub>2</sub> O <sub>6</sub> ] Properties . . . . .	6
1.3	Liquid Water Properties . . . . .	8

---

\*To whom correspondence should be addressed

<sup>†</sup>CNR-ISM

<sup>‡</sup>University of Udine

<sup>¶</sup>CNR-IOM DEMOCRITOS

<sup>§</sup>Università de L'Aquila

1.4	Structural and Dynamical Properties of Solvated Clusters in DFT+U and DFT-D2 AIMD Simulations . . . . .	9
1.5	Optimized Geometries of the c1 and c2 Clusters and Details of the employed Co, O and H Pseudopotentials . . . . .	12
<b>2</b>	<b>Ab Initio Molecular Dynamics Simulations</b>	<b>16</b>
2.1	c1 cluster . . . . .	16
2.2	c2 cluster . . . . .	19
2.3	c3 cluster . . . . .	21
<b>3</b>	<b>Oxidation Potential of the CoCat Model</b>	<b>22</b>

## 1 Assessment of Theoretical Methods

Four different systems have been investigated in order to provide evidence that our DFT+U setup represents an accurate and reliable approach to investigate the reaction pathways promoted by the CoCat: (i) the  $\text{LiCoO}_2$  results indicate that both the  $\text{Co(III)O}_6$  bonds and the  $\text{Co}(3d)\text{-O}(2p)$  mixing are well reproduced by the present DFT+U calculations; (ii) the  $[\text{Co(II)}(\text{H}_2\text{O})_6]$  DFT+U results indicate that our setup describes in a correct way the interplay between the electronic levels of water molecules and the  $3d$  orbitals of Co ions; (iii) the vibrational properties of liquid water suggest the reliability of our DFT+U framework when applied to reaction pathways involving water molecules; (iv) finite temperature effects, as well as dispersion contributions, have been checked by comparing AIMD simulations of solvated c1 clusters with X-ray absorption spectroscopy measurements, thus extending our previous results.<sup>1</sup> Finally, the optimized geometries of the c1 and c2 clusters, together with the Co, O and H pseudopotentials used in the simulations, are provided in order to ensure a full reproducibility of our results.

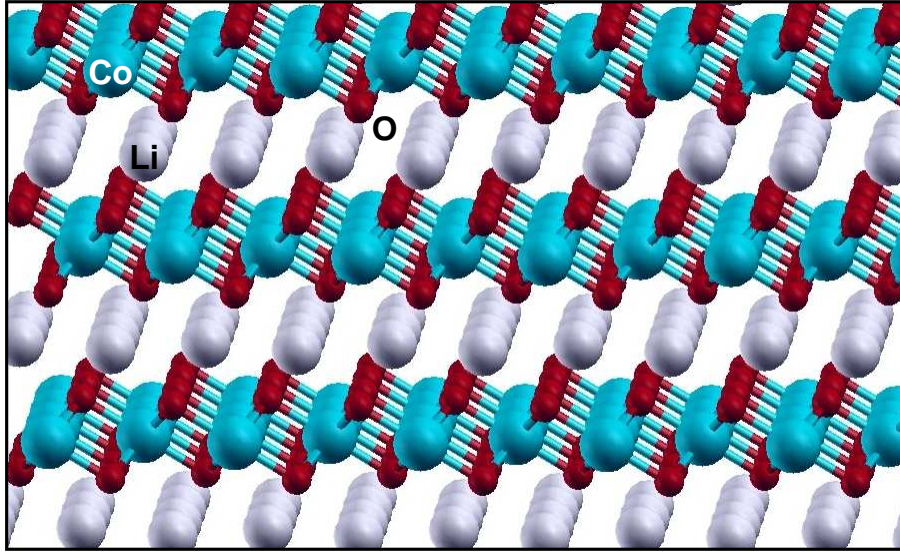


Figure S1: Structure of the layered  $\text{LiCoO}_2$  bulk crystal. Layers of Li atoms are intercalated between  $\text{CoO}_2$  layers formed by  $\text{Co(III)O}_6$  octahedra.

Table SI: **Structural properties of the  $\text{LiCoO}_2$  crystal.** Theoretical DFT(PBE) results (obtained by using ultrasoft (US) and norm conserving (NC) pseudopotentials), and DFT+U results are compared with XRD measurements.<sup>2</sup> The Co-O column is related to nearest neighbour Co and O atoms. The Co-Co 1 label denotes the distance between Co-Co nearest neighbours separated by a  $\mu$ -oxo bridge; Co-Co 2 is the shortest distance between two Co atoms which are not directly connected by a  $\mu$ -oxo bridge, and Co-Co 3 is the distance between the far atoms in three collinearly arranged Co atoms.

Structure [Method]	Bond Distance ( $\text{\AA}$ )			
	Co-O	Co-Co 1	Co-Co 2	Co-Co 3
$\text{LiCoO}_2$ [DFT (PBE-US)]	1.935	2.848	4.932	5.695
$\text{LiCoO}_2$ [DFT (PBE-NC)]	1.935	2.840	4.919	5.680
$\text{LiCoO}_2$ [DFT+U(Co)]	1.941	2.843	4.924	5.685
$\text{LiCoO}_2$ [DFT+U(Co,O)]	1.925	2.829	4.900	5.659
$\text{LiCoO}_2$ XRD data	1.92(5)	2.816(6)	4.878(5)	5.633(2)

## 1.1 LiCoO<sub>2</sub> Properties

To assess the capability of our *ab initio* calculation to predict Co-O and Co-Co distance at sufficient precision, we have investigated a crystallographically (XRD) characterized Co-oxo compound with close structural similarity to the CoCat, namely LiCoO<sub>2</sub>. This material consists of Co-O sheets of interconnected incomplete cubane units (layers of edge-sharing Co(III)O<sub>6</sub> octahedra) separated by intercalated Li<sup>+</sup> ions (Figure S1). In detail, we validated our theoretical setting by performing simulations of the LiCoO<sub>2</sub> properties by using a 12-atom hexagonal supercell. Satisfactorily converged results were achieved by using a  $8 \times 8 \times 4$  **k**-point mesh and the same 40/320 Ry cutoffs used in the case of the CoCat simulations. Concerning the structural properties of the LiCoO<sub>2</sub>, we have estimated lattice parameters values at the DFT(PBE) level ( $a=2.848$  Å and  $c=14.025$  Å) in close agreement with experimental ones ( $a=2.816$  Å and  $c=14.044$  Å).<sup>3</sup> An even closer agreement have been achieved in the case of DFT+U(Co,O) results ( $a=2.829$  Å and  $c=14.090$  Å). A further set of DFT(PBE) simulations have been carried out by using norm-conserving Martins-Troullier pseudopotentials<sup>4</sup> and 140/560 Ry cutoffs in order to show that the achieved results are not biased by the choice of a particular kind of pseudopotential. A final set of simulations has been carried out at an accurate hybrid Hartree Fock/DFT level, by using the Heyd-Scuseria-Ernzerhof HSE06 exchange-correlation functional.<sup>5,6</sup> Only in the case of such a computationally expensive approach, the above norm-conserving pseudopotentials and 140/560 Ry cutoffs have been used to perform a geometry optimization of the LiCoO<sub>2</sub> crystal at the XRD lattice parameters.

Table SI provides a comparison of distances obtained experimentally (by XRD measurements<sup>2</sup>) and calculated by the above different *ab initio* approaches. Experimentally determined and calculated distances agree reassuringly well. Using the DFT+U approach, the deviations are around 0.02 Å; slightly more pronounced deviations were observed in the DFT (PBE) simulations. It has to be noted that in the case of DFT+U(Co) results, an excessive softening of the Co-O bonds has been found, in agreement with similar calculations performed by using a DFT+U(Ti) approach in the case of TiO<sub>2</sub>.<sup>7</sup> An optimally balanced correction applied to both Co (*3d*) and O(*2p*) shells (DFT+U(Co,O) framework) is able to reproduce quite accurately the measured Co-O distance, as

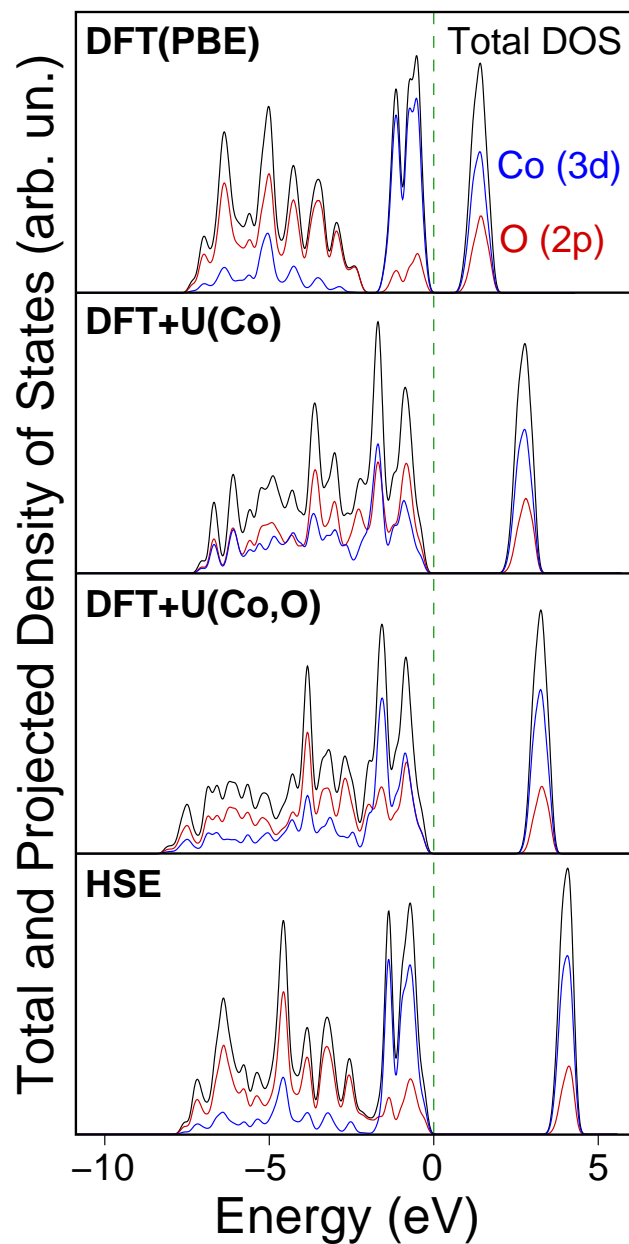


Figure S2: Total (black lines) and Projected on O(2p) (red lines) and Co(3d) (blue lines) atomic orbitals DOS (density of states) of the layered LiCoO<sub>2</sub> bulk crystal, investigated at different levels of the theory (see the text). A zero energy value has been assigned to the valence band maximum in all the cases.

shown by a comparison of the values of the Co-O column in Table SI.

On the side of the electronic properties, the DFT(PBE) approach underestimates the Kohn-Sham energy gap: a value of 1.1 eV has to be compared to the experimental value of  $2.7 \pm 0.3$  eV.<sup>8</sup> Moreover, the strong hybridisation between O( $2p$ ) and Co( $3d$ ) orbitals, reported on the ground of photoemission electron spectroscopy measurements,<sup>9</sup> is only slightly appreciable at a DFT(PBE) level, as shown by the corresponding projected Density Of States (pDOS) in Figure S2. Both these issues result to be improved in the case of both DFT+U calculations: a strong O( $2p$ )-Co( $3d$ ) mixing is clearly shown by the pDOS in Figure S2 and an energy gap value of 3.0 eV (2.5 eV) in the case of DFT+U(Co,O) (DFT+U(Co)) calculations nicely approaches the experimental value, while a significant overestimation (3.9 eV) of the energy gap value is reported in the case of hybrid HSE calculations.

## 1.2 [Co(II)H<sub>2</sub>O<sub>6</sub>] Properties

The [Co(II)(H<sub>2</sub>O)<sub>6</sub>] coordination complex has been chosen to elucidate the fine interplay between the Hubbard U corrections applied to the Co( $3d$ ) atomic orbitals and to the O( $2p$ ) atomic orbitals. The achieved results, in turn, allows us to justify the choice of the DFT+U(Co,O) setup in the case of the CoCat simulations discussed in the main text. In detail, the [Co(H<sub>2</sub>O)<sub>6</sub>]<sup>2+</sup> ion have been accommodated in a large (26 Å<sup>3</sup>) cubic supercell, and the Martyna-Tuckerman method<sup>10</sup> has been used to correct for the spurious long-range interactions between periodically repeated images. Four electronic structure levels of calculations have been considered: DFT(PBE), DFT+U(Co) and DFT+U(Co,O) methods have been described in the main text; HSE calculations have been performed by using the same setup discussed in the case of LiCoO<sub>2</sub> results. Keeping in mind that we are interested in a validation of our computational setup in the case of the CoCat calculations, we have not recalculated a self consistent value for the Hubbard U correction of Co( $3d$ ) atomic orbitals in the [Co(II)(H<sub>2</sub>O)<sub>6</sub>] system. We are thus applying the 5.9 eV value calculated in the case of the CoCat simulations. We focus on the electronic eigenvalues of the stable high-spin [Co(II)(H<sub>2</sub>O)<sub>6</sub>] system, which are presented in Figure S3 in form of a spin-polarised total and projected on Co( $3d$ )

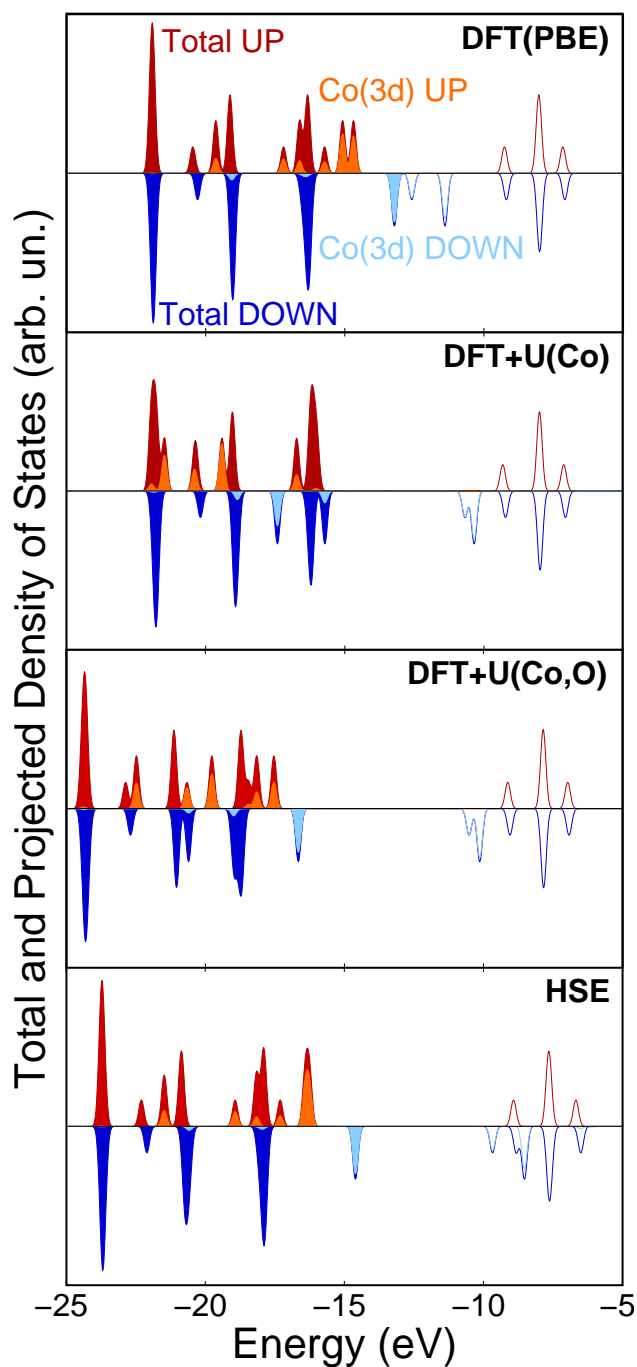


Figure S3: Spin polarised (UP and DOWN) total (dark red and dark blue lines, respectively) and projected on Co(3d) atomic orbitals (orange and light blue lines, respectively) DOS (density of states) of an isolated  $[\text{Co}(\text{II})(\text{H}_2\text{O})_6]$  species, investigated at different levels of the theory (see the text). A 0.01 Ry (0.14 eV) Gaussian broadening of electronic eigenvalues has been applied to simulate a DOS in order to clarify the spin up and spin down Co(3d) contributions to the molecular orbitals. Filled (non filled) curves indicate occupied (unoccupied) molecular orbitals.

density of states. Such a graphical description allows one to frame at a glance the positions in energy of the 5 majority and 2 minority Co(3d) electrons and their relationships with the ligand orbitals. Plain DFT(PBE) calculations are characterised by a very small gap (0.6 eV, in the spin down channel) between occupied and unoccupied states, in agreement with the strong delocalisation error expected in the case of atomic-like orbitals.<sup>11,12</sup> A Hubbard U correction applied to the Co(3d) electrons only, as often used in the case of transition metals interacting with organic ligands,<sup>13,14</sup> opens a wider gap between Co(3d) orbitals, as shown by the DFT+U(Co) plot. However, a dramatic qualitative change occurs in the ordering of frontier orbitals, the highest occupied orbitals in both spin up and spin down channels being now ligand orbitals. This implies the fact that an electron subtracted from the  $[\text{Co}(\text{H}_2\text{O})_6]^{2+}$  system would be drained from the ligands rather than from the Co(II) center. A more reasonable orbital line-up is retained instead when an U correction is applied to both the Co(3d) and O(2p) shells, which is also in good agreement with the results of the HSE calculations (compare the DFT+U(Co,O) and HSE plots in Figure S3).

### 1.3 Liquid Water Properties

Our double DFT+U(Co,O) correction has been already validated in the case of the properties of several metal oxides including, apart from the above LiCoO<sub>2</sub> results, TiO<sub>2</sub> and ZnO.<sup>7,15</sup> We have performed two sets of DFT(PBE) and DFT+U(O) calculations of liquid water at 300 K in order to show that our 5.9 eV Hubbard U correction applied to the O(2p) orbitals is not detrimental to the properties of liquid water with respect to the well investigated DFT(PBE) approach.<sup>16</sup> In this regard, 32 water molecules have been accommodated in a 9.869 Å<sup>3</sup> box. After 5 ps of thermal equilibration of the system, a 13 ps NVT simulation has been performed by using the same setup described in the case of the CoCat simulations. First, the density of vibrational modes (DVM) of the investigated systems have been obtained by extracting power spectra out of the velocities autocorrelation functions. DVM plots obtained in the case of DFT(PBE) and DFT+U(O) simulations are shown in the inset of Figure S4. Simulated vibrational spectra have been obtained by weighting such DVM plots with the oscillator strengths calculated by applying the linear response

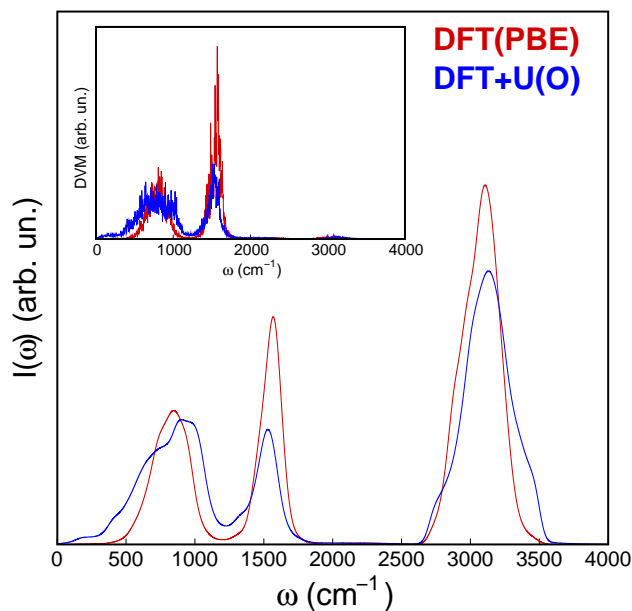


Figure S4: Simulated IR spectra of liquid water, obtained by using the DFT(PBE) and DFT+U(O) methods described in the text. The related densities of vibrational modes (DVM) extracted from ab initio molecular simulations are shown in the inset.

method described in Ref. 17 to the same system. The achieved results show that both applied approaches reproduce quite well the three main features of the water infrared absorption: a broad low-frequency peak related to intermolecular bending and stretching modes, a sharp feature related to the intramolecular bending mode, peaked at  $1645 \text{ cm}^{-1}$ , a feature related to the symmetric and asymmetric stretching modes, peaked at about  $3300 \text{ cm}^{-1}$  and widely broadened by intermolecular H bond effects.<sup>18</sup>

## 1.4 Structural and Dynamical Properties of Solvated Clusters in DFT+U and DFT-D2 AIMD Simulations

In our previous contribution,<sup>1</sup> the structural properties of the c1 and c2 CoCat models obtained by AIMD simulations at the DFT(PBE) level and static simulations at the DFT(PBE) and DFT+U levels were compared with the results of X-ray absorption (XAS) measurements. Such a comparison were also extended to the effects of proton mobility on the Co-Co distances. We complete here that investigation by presenting the results of further AIMD simulations of the solvated c1

Table SII: Structural properties extracted by DFT(PBE), DFT(PBE)+D2, DFT+U, DFT+U+D2 AIMD simulations of the solvated c1 cluster (see the text). The Co-O column is related only to Co-O bonds belonging to the cubane structures. The Co-Co 1 label denotes the distance between nearest neighbours separated by a  $\mu$ -oxo bridge; Co-Co 2 is the shortest distance between two Co atoms which are not directly connected by a  $\mu$ -oxo bridge, and Co-Co 3 is the distance between the far atoms in three collinearly arranged Co atoms. Data have been averaged on different bonds of the same type and along the trajectory. CoCat XAS data are taken from Risch et al.<sup>19</sup>

Method	Bond Distance (Å)			
	Co-O	Co-Co 1	Co-Co 2	Co-Co 3
DFT(PBE)	1.91±0.05	2.84±0.06	4.77±0.16	5.65±0.08
DFT(PBE)+D2	1.91±0.05	2.84±0.06	4.78±0.20	5.68±0.07
DFT+U	1.91±0.04	2.84±0.05	4.74±0.19	5.64±0.07
DFT+U+D2	1.91±0.04	2.85±0.05	4.75±0.22	5.66±0.05
CoCat XAS data	1.89	2.81	4.86	5.62

cluster at 300 K performed at the DFT+U level, as well as by adding a semiempirical DFT-D2 dispersion correction<sup>20</sup> to both DFT(PBE) and DFT+U AIMD simulations. All the systems have been restarted from ion positions and velocities obtained by the previous DFT(PBE) run, thermalized for 2 ps, and then propagated for further 5 ps. The structural properties extracted by such AIMD simulations are reported in Section 2. In all the investigated cases the results are in a good agreement with both previous DFT(PBE) simulations,<sup>1</sup> and XAS measurements.<sup>19</sup>

The motion of protons at the CoCat/water interface represents one of the keys for the CoCat functioning, as discussed in the main texts. We have performed a more detailed analysis of our AIMD results in order to verify that the application of a DFT-D2 dispersion correction does not affect the results of our simulations, thus strengthening our theoretical setup and our main results related to the oxygen evolution mechanism. As a significant example, our previous DFT(PBE) results related to the fast motion of a H<sup>+</sup> ion across one of the low-barrier H bonds characterizing the catalyst boundaries,<sup>1</sup> are in full agreement with the results extracted from the above DFT(PBE)+D2 simulation, shown in Figure S5.

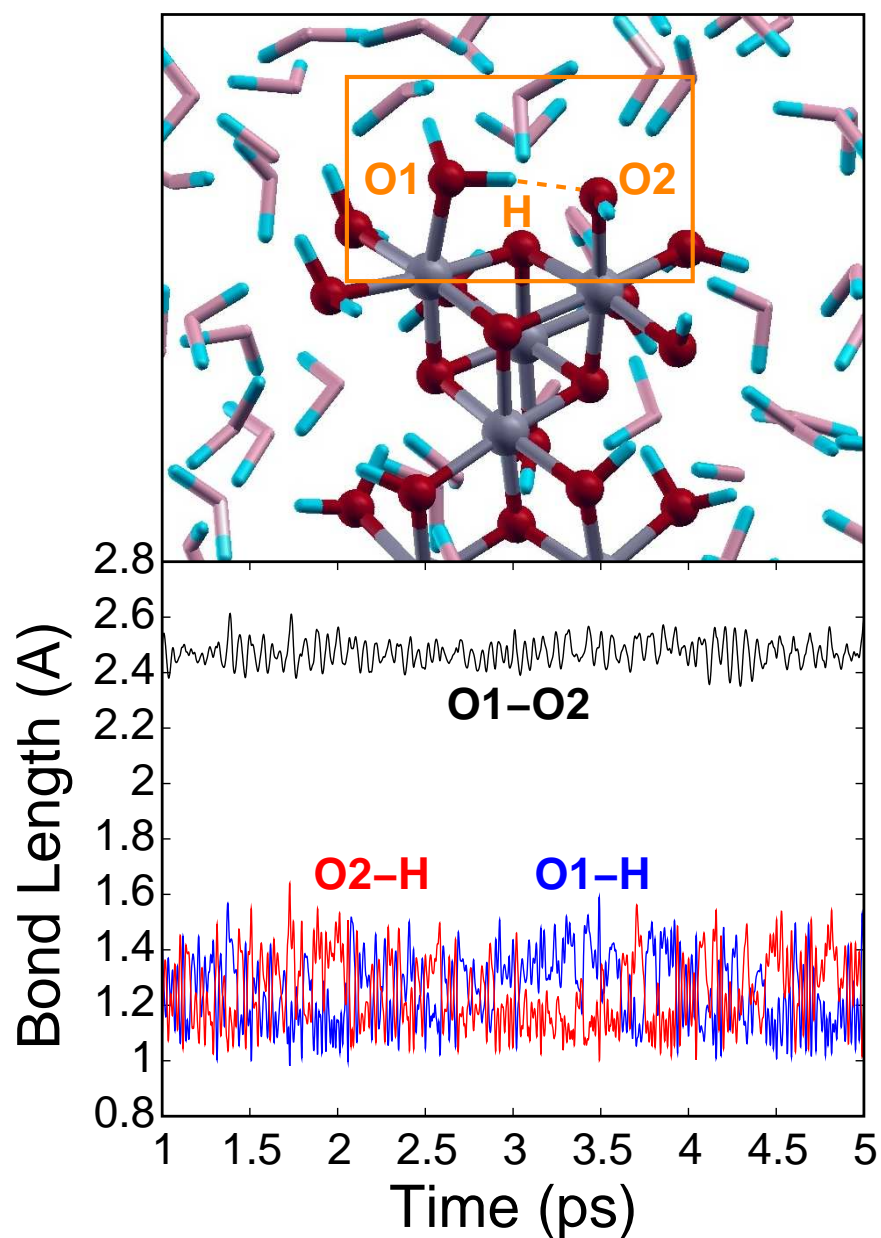


Figure S5: Upper panel: snapshot from the DFT(PBE)+D2 simulation of the c2 model in water solution. The orange ellipse identifies a pair of terminal O atoms which undergoes a fast proton exchange along the simulation. O atoms belonging to surrounding water molecules have been displayed in a lighter red colour for the sake of clarity. Lower panel: evolution of atomic distances related to the H-O-H $\cdots$ O-H structure along the DFT(PBE)+D2 simulation.

## 1.5 Optimized Geometries of the c1 and c2 Clusters and Details of the employed Co, O and H Pseudopotentials

Optimized geometry (in cartesian coordinates, Å units) of the  $\text{Co}_6\text{O}_{23}\text{H}_{28}$  c1 cluster

```
Co 2.024213738 2.224420292 4.034294234
Co 2.086125058 3.917008942 1.854163975
Co 4.120703658 2.048639182 2.073740181
Co 4.040573999 4.124129536 3.903676424
Co 5.737161934 3.866091296 6.104737696
Co 3.796244376 5.943985632 6.024618362
O 2.223050095 2.089427278 2.192848845
O 2.145833509 4.076596229 3.747379022
O 3.928346723 2.206283440 3.965218655
O 3.947270183 3.898273064 2.026505032
O 2.056360839 2.489501462 5.999866432
O 1.993684816 0.207305191 4.337828567
O 0.101278012 2.385231621 3.930644346
O 0.098315876 3.733409976 1.902924070
O 2.114068902 5.888729868 1.235801401
O 2.220870835 3.753595658 -0.072555460
O 4.529946921 0.044852969 2.228317320
O 6.045560221 1.966089044 2.202205655
O 4.014627582 2.025175879 0.114823374
O 3.940727488 4.085260082 5.795028763
O 5.941135717 4.026243241 4.217715297
O 4.086399939 6.024989741 4.144222332
O 5.722055220 5.786849602 6.241834556
O 7.677274364 3.679351803 6.614519535
```

O 5.470886774 1.940840964 5.834230042  
O 5.552787242 3.849128630 8.025140965  
O 1.860231020 5.760038882 5.659476538  
O 3.559003815 7.756905324 6.335282573  
O 3.644352395 5.599748220 7.965783027  
H 5.993036081 6.115077552 7.107560196  
H 2.877917562 3.159422219 6.081023968  
H 1.836009667 0.009686442 5.272158682  
H 1.483081952 -0.335811646 3.722738735  
H 1.239088483 2.926930051 6.277685165  
H -0.434284227 1.587008235 3.943463553  
H -0.018582894 3.114139662 2.807464490  
H -0.491852620 4.493114526 1.905322535  
H 3.505405442 6.548143287 3.580836475  
H 1.353738774 6.480038896 1.247272866  
H 2.252493850 5.460141751 0.345029895  
H 1.407423777 3.374860008 -0.427468441  
H 4.250289359 -0.261235997 3.101317013  
H 5.469601520 0.399144793 2.233728742  
H 6.235517292 3.251132416 3.692567888  
H 6.547728609 2.503749427 1.582096553  
H 4.837626233 2.137741748 -0.371614958  
H 3.297276883 2.761965050 -0.099002001  
H 8.230025446 4.389436768 6.260975388  
H 6.282517099 1.447347766 5.665988436  
H 4.765062874 1.934242146 4.964135831  
H 7.424114075 3.796889527 7.559605553

H 5.252739432 2.985936150 8.335736262  
H 1.518402969 6.661208324 5.579592274  
H 1.785245559 5.150039198 4.833174561  
H 4.193222731 8.295978013 5.851485145  
H 4.378466411 4.921487313 8.185691885  
H 3.663855160 6.444785085 8.434691202

**Optimized geometry (in cartesian coordinates, Å units) of the Co<sub>7</sub>O<sub>24</sub>H<sub>27</sub> c2 cluster**

Co 1.438231228 5.456230911 2.363821018  
Co 2.939764913 3.119916683 2.345619177  
Co 4.246101414 5.600517054 2.328093264  
Co 2.746772410 7.950221087 2.358897073  
Co 5.726268430 3.239933908 2.314667647  
Co 7.057551315 5.741375084 2.282442209  
Co 5.531097080 8.091604785 2.299225909  
O 1.508968567 2.148984782 3.276150288  
O 1.660492873 3.940533952 1.155703049  
O 0.164166782 4.332174912 3.421557027  
O -0.051059966 6.391176710 1.347247594  
O 1.453631878 7.030465488 3.472225014  
O 1.195602732 8.993109282 1.398728914  
O 2.827106000 1.249043864 1.393276523  
O 4.394509063 2.511384165 3.517212677  
O 4.309903706 3.917592489 1.374282668  
O 2.849326222 4.690028536 3.281275429  
O 2.734305230 6.356469280 1.401827542  
O 4.176280418 7.247007824 3.271491119

O 4.067019129 8.680029994 1.174700316  
O 2.669615082 9.680276633 3.282319257  
O 5.630890137 1.465252212 1.279609681  
O 7.161885410 2.355096762 3.561902274  
O 6.997096677 4.109845481 1.169566138  
O 5.746212866 4.806280452 3.260298658  
O 5.626412775 6.478406810 1.376554253  
O 6.836537546 7.256469367 3.476772404  
O 6.990625455 8.791134488 1.197367055  
O 5.250979726 9.796898680 3.325584289  
O 8.533576897 4.924260672 3.409647105  
O 8.333305589 6.778994357 1.292484962  
H 0.556960718 3.385799358 3.399451947  
H 1.763425872 1.877617380 4.166194047  
H -0.769288829 4.380125329 3.186839782  
H 0.151160597 7.351644471 1.424125004  
H -0.108590283 6.117309398 0.422691444  
H 1.544850609 9.295166105 0.547845561  
H 2.137915234 1.206231363 2.154383423  
H 4.683739792 1.185258722 1.310042861  
H 5.933770414 1.575323625 0.368929438  
H 4.226904365 9.896046971 3.345853903  
H 2.283843849 9.612265612 4.163225286  
H 5.627566334 9.770480834 4.212766030  
H 8.143482698 4.197760702 3.925551834  
H 8.916965724 5.632043844 3.945234066  
H 6.512589202 1.884748972 4.114966710

H 7.698384519 7.945122566 1.155868744  
H 7.359864645 9.628782802 1.495283267  
H 8.687821884 6.342269481 0.511966011  
H 2.221723524 4.321114896 0.458768355  
H 4.155837892 8.106948254 0.397941232  
H 6.511779109 4.409948335 0.385524185  
H 1.857542662 6.780179838 4.314965264  
H 4.327569762 3.176788060 4.223517443  
H 6.287329598 6.904292704 4.195764885  
H 1.515369534 9.625789483 2.132921086  
H 7.718039324 1.731664861 3.072498249  
H 2.365268171 1.364373997 0.550366037

The Co\_pbe-sp-van.UPF, O\_pbe.van.UPF and H\_pbe.van.UPF ultrasoft pseudopotentials can be downloaded from the Quantum ESPRESSO online pseudopotential library:

<http://www.quantum-espresso.org/pseudopotentials/>

## 2 Ab Initio Molecular Dynamics Simulations

### 2.1 c1 cluster

The c1 cluster is formed by one complete and one incomplete cubane-like units, connected by a single Co vertex. Its structural properties are in close agreement with EXAFS measurements of the CoCat, as detailed in the main text. Molecular dynamics simulations and corresponding paths were considered as discussed in the following.

**Simulation (I).** No significant structural changes were observed before the removal of the 4<sup>th</sup> electron from the Co<sub>6</sub>O<sub>23</sub>H<sub>24</sub> cluster. 0.8 fs after such removal, one of the terminal Co-OH groups of

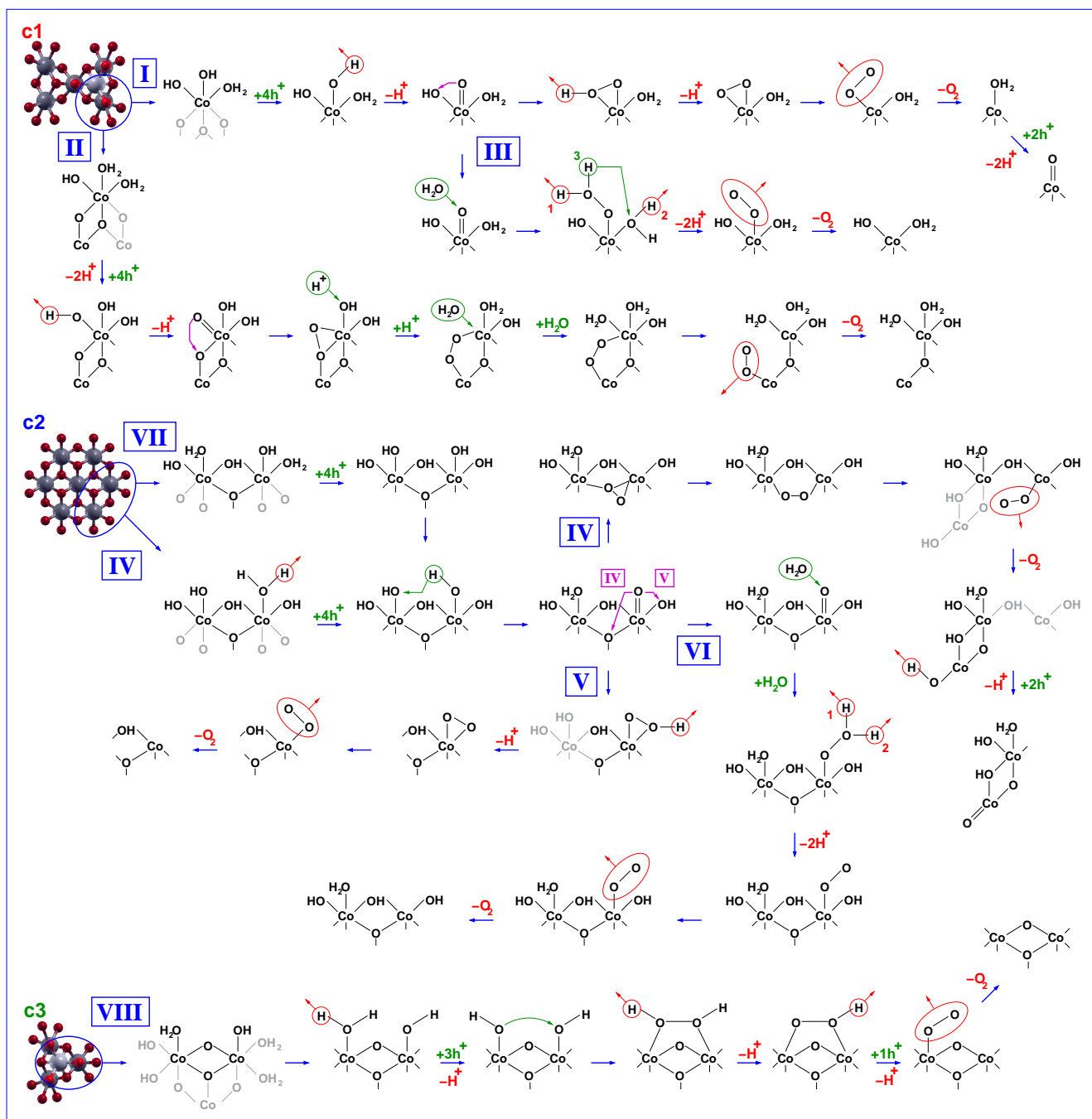


Figure S6: Detailed AIMD paths for oxygen evolution promoted by the c1 (I-III), c2 (IV-VIII) and c3 (VIII) CoCat models. A description of each path is discussed in Sections Section 2.1, Section 2.2 and Section 2.3.

the complete cubane-like unit releases its  $H^+$  into the solution leaving back a **Co=O oxyl radical**. The Co=O species was not stable and evolves after 1.1 ps towards a **Co(OOH) hydroperoxo** intermediate by means of geminal coupling with a neighboring terminal Co-OH group. The Co(OOH) releases a further  $H^+$  ion after 1.4 fs, thus forming a **Co(O<sub>2</sub>) peroxo** intermediate, which after 1.8 ps breaks one of the Co-O bonds resulting in a **Co-O-O superoxo** group. This last configuration was highly stable (up to 10 ps dynamics) unless the total spin state of the system is switched from singlet to triplet to promote dioxygen release in triplet state. The relevant energy gain of the O<sub>2</sub> molecule, when switched from singlet to triplet state, is sufficient to promote an almost immediate breaking of the Co-O bond and the release of O<sub>2</sub>. The four-fold coordinated Co atom remained under-coordinated still for 5 ps simulated time, suggesting that this saturation process occurs on a slower time scale. To evaluate the height of the energy barrier for H<sub>2</sub>O/Co rebound static NEB calculations were performed, providing an estimate of 0.3 eV. The injection of two additional  $h^+$  in the system induces the formation of a new Co=O oxyl species, thus suggesting that the catalyst does not need to be brought back to its initial, resting conditions after every single release of an O<sub>2</sub> molecule. The formation of Co=O radicals located in different positions of the same cluster, upon loading of further  $h^+$ , suggests that further O atoms may be scavenged from the catalyst, in agreement with the results of isotopic labelling experiments indicating,<sup>21</sup> until self-repairing mechanisms of the CoCat<sup>22,23</sup> promote competing parallel processes in order to recover the original stoichiometry.

**Simulation (II).** In order to investigate whether the choice of H saturation of our model, as well as variations in the background passivation of charged supercells, might affect the observed reaction mechanism, we added two more H atoms to the previous system (Co<sub>6</sub>O<sub>23</sub>H<sub>26</sub> cluster). To start the simulation with a cluster containing all Co (III) ions, the total charge of the system is therefore changed accordingly. The high mobility of  $H^+$  ions at the cluster/solution interface<sup>1</sup> permits again the occurrence of terminal Co-OH groups on one of the Co vertices of the complete cubane-like unit. This, in turn, permits the localization of holes (as discussed in the main text) and the formation of a **Co=O oxyl radical**, 650 fs after the removal of the 4<sup>th</sup> electron from the system. At variance

with Path (I), the unstable Co=O group forms a different **Co-O-O-Co peroxy** group after 1.4 ps by means of geminal coupling with an internal  $\mu_3$ -O atom (see Figure 1 in the main text). The Co-O-O-Co intermediate evolves towards a **Co-O-O superoxy** group, and towards the release of an O<sub>2</sub> molecule, when the spin state is switched to triplet.

**Simulation (III).** The **Co=O oxyl radical** of Path (I) is forced to undergo a nucleophilic attack promoted by an external water molecule. In practice, this is accomplished by rotating "on-the fly" the nearest water molecule, with the O atom pointing towards the Co=O group. All of the nuclear velocities are conserved, but the ones related to the rotated water molecules, which are set to zero. This allows an immediate formation of a stable O-O bond, followed by the fast release of two H<sup>+</sup> ions ((H)<sub>1</sub> and (H)<sub>2</sub> in Figure S6), which is already accomplished 200 fs after the O-O bond formation. The resulting **Co(OOH) hydroperoxy** intermediate exchanges a further H<sup>+</sup> ions ((H)<sub>3</sub> in Figure S6) with a geminal Co-OH group, thus evolving towards a **Co-O-O superoxy** group only 500 fs after the formation of the O-O bond. Once again, the switching of spin state induce the release of an O<sub>2</sub> molecule. An high potential energy barrier (1.0 eV) has been estimated in the case of the first step of this reaction path, as discussed in the main text.

## 2.2 c2 cluster

The c2 cluster has been cut out from a single Co-O sheet of the LiCoO<sub>2</sub> crystal, that is, a solid long-range ordered system showing close similarities to the building blocks of the amorphous CoCat.<sup>1,24</sup> It is formed by incomplete cubane-like units only, sharing edges, and its structural properties are again in close agreement with EXAFS measurements of the CoCat. At variance with the c1 cluster, the occurrence of a regular distribution of pairs of parallel terminal Co-O bonds, generally coupled by low barrier H-O-H...O-H bonds,<sup>1</sup> plays a key role both in the fast motion of H<sup>+</sup> ions across the catalyst and in a sort of "self regulation" of the H saturation of the cluster boundaries, less flexible than that reported in the case of cluster c1 (see the comments to Simulation (VII)).

**Simulation (IV).** A solvated Co<sub>7</sub>O<sub>24</sub>H<sub>24</sub> cluster was considered and the removal of the first three electrons proceeded without significant structural changes. The breaking of one of the H-O-H...O-

H structures after the removal of the third electron from the cluster represents a preliminary step to the release of one  $H^+$  ion to the solution, taking place 500 fs after the removal of a fourth electron from the system by means of a  $H^+$  transfer induced by the low barrier H bond with the parallel Co-OH group. The **Co=O oxyl radical** formed is a stable intermediate in the case of the c2 cluster, as detailed in the main text. It evolves spontaneously after 1.1 ps by crossing a small potential energy barrier towards the formation of a **Co-O-O-Co peroxy** group, similar to the Simulation (II) one, by means of geminal coupling with an internal  $\mu_3$ -O atom. Such an inner peroxy group is quite stable and breaks up only by switching the spin state to triplet, leading to the fast formation of a **Co-O-O superoxy** group and to the release of an  $O_2$  molecule. The ignition of further  $h^+$  in the system induces the release of  $H^+$  ions and the formation of a new Co=O oxyl radical, as already discussed in the case of Simulation (I).

**Simulation (V).** A slight displacement of the O atom involved in the formation of the Co=O radical has been induced to promote the formation of a terminal **Co(OOH) hydroperoxy** group instead of an inner Co-O-O-Co peroxy group. A low 0.2 eV potential energy barrier has been estimated for such a reaction step, as discussed in the main text. The hydroperoxy intermediate loses a  $H^+$  ion after 400 fs, thus leading to the formation of a **Co(O<sub>2</sub>) peroxy** intermediate. The switching to the triplet spin state induces the fast formation of a **Co-O-O superoxy** group and the release of an  $O_2$  molecule.

**Simulation (VI).** Starting from the oxyl species of Simulation (IV), in a way similar to the one discussed in the case of Simulation (III), one external water molecule has been forced to form a O-O bond with the Co=O radical. The following reaction path is quite fast and straightforward to the formation of a **Co-OOH hydroperoxy** group (300 fs after the formation of the O-O bond), and of a **Co-O-O superoxy** group (1.1 ps after the formation of the O-O bond). The last intermediate releases the  $O_2$  molecule when the system is switched to the triplet spin state. An estimate of the high energy barrier of the first step of this reaction path (1.0 eV) is discussed in the main text.

**Simulation (VII).** The dynamics show the peculiar nature of low barrier H bonds related to the presence of parallel Co-O bonds, with the two O atoms placed at a distance of about 2.8 Å. This

conformation is responsible for the occurrence of quite stable H-O-H...O-H structures continuously exchanging one H<sup>+</sup> ion.<sup>1</sup> Two H atoms were added to the Co<sub>7</sub>O<sub>24</sub>H<sub>24</sub> cluster used in Simulations (IV-VI) in order, once again, to ensure that a particular choice of H saturation does not significantly affect the reaction mechanism. This addition leads to the formation of unstable pairs of H<sub>2</sub>O molecules bonded to neighbouring Co atoms, instead of the stable H-O-H...O-H configuration. During the removal of electrons from the system, two H<sup>+</sup> ions are released indeed in the solution, thus recovering the stable configuration already discussed in the Simulation (IV) case.

### 2.3 c3 cluster

The smallest considered system, the c3 cluster, is formed by a single complete cubane-like unit. This model has been already used in a first mechanistic study of the CoCat induced formation of an O-O bond,<sup>25</sup> performed by using a QM/MM approach. It may be also considered as a model for metallo-organic homogeneous catalysts containing cubane-like Co-O<sup>26,27</sup> (Mn-O,<sup>28,29</sup> Ni-O<sup>30</sup>) structures. In our previous study we did not take into account this smaller cluster since it contains only nearest neighbours Co-Co pairs and therefore it cannot account for the CoCat XAS measurements.

**Simulation (VIII).** One of the H-O-H...O-H structures is broken during the removal of electrons from the cluster, by forming two parallel Co-OH terminal groups. This leads to the formation of a **bridging Co-OH-OH-Co** group 400 fs after the removal of the third electron from the system. This is the only case in which the O-O bond does not form spontaneously by coupling of geminal O atoms. The Co-OH-OH-Co intermediate loses one H<sup>+</sup> ion 200 fs later, thus evolving towards a **bridging hydroperoxo Co-O-OH-Co** group which is stable until the removal of a fourth electron from the system. The Co-O-OH-Co group loses one further H<sup>+</sup> ion and breaks one of the Co-O bonds immediately after the removal of such electron, forming a **Co-O-O superoxo** group which release an O<sub>2</sub> molecule when the system is switched to the triplet spin state. Regarding the single exception represented by the reaction mechanism identified in the case of this simulation, it has to be noted that the breaking of a H-O-H...O-H induces the localization of holes on both the resulting

parallel Co-OH groups. In our opinion, this should be considered as an artifact due to too small dimensions of the c3 cluster, a single cubane-like unit in which all of the Co atoms are nearest neighbours of each others. The repulsion of holes leads to their localization on different cubane-like units in the c1 and c2 clusters, as discussed in the main text. The structural properties of the CoCat, basically an amorphous solid-state Co oxide, suggest that a trend can be extrapolated beyond the dimension of the present clusters, indicating a wider distribution of oxidizing holes across the catalyst surface.

### 3 Oxidation Potential of the CoCat Model

The electrochemical properties of a solid-state extended electrode, acting as a catalyst for oxygen evolution, have been simulated by using a series of H-saturated Co-O clusters. We have already shown that our cluster models, together with our theoretical setup, account for all the known measured structural and electronic properties of the CoCat. In this section we discuss our estimate of the oxidation potentials of the c1 cluster provided in the main text, in agreement with the external potential promoting the CoCat-based oxygen evolution (1.18 V vs SHE).<sup>21</sup> We have used to this purpose a robust technique, generally employed to the estimate of potential energy levels of dopant and defects in the framework of the simulations of the electronic properties of semiconductors.<sup>31</sup> The same approach has been also successfully used to investigate the reduction of oxygen molecules promoted by a photoactivated TiO<sub>2</sub> surface.<sup>32,33</sup>

In general, the formation energy  $\Omega_f$  of a  $q$ -charged species  $M$ , considered as a defect or dopant in a dielectric host  $H$ , e. g., a semiconductor lattice, is defined as

$$\Omega_f[M^q] = E[M^q] - E[H] - \sum n_M \mu_M + q(\epsilon_F + \epsilon_{\text{VBM}}) \quad (1)$$

where  $E[H]$  and  $E[M^q]$  are the total energies of supercells containing the undoped and the doped host lattice, respectively,  $n_M$  is the number of metal atoms in the defected supercell and  $\mu_M$  is the chemical potential of the same species.  $\epsilon_F$  is the Fermi level of the system, referenced to

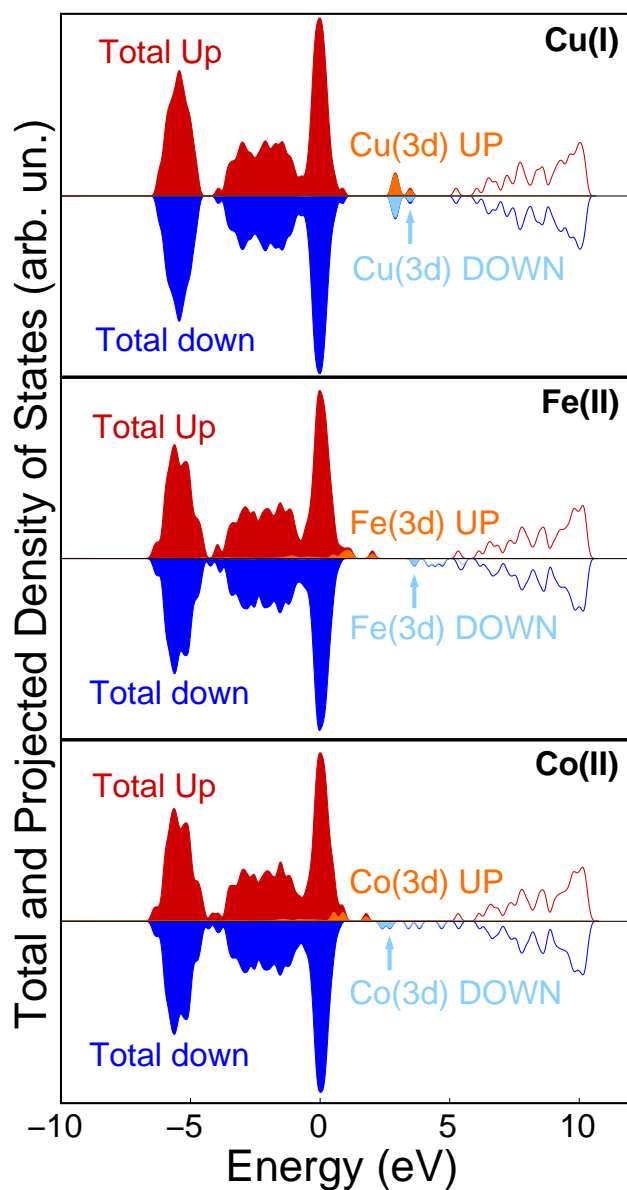


Figure S7: DFT(PBE) Spin polarised (UP and DOWN) total (dark red and dark blue lines, respectively) and projected on Cu(3d), Fe(3d) and Co(3d) atomic orbitals (orange and light blue lines, respectively) DOS (density of states) of a Cu(I) (Fe(II), Co(II)) ion in an explicit water environment. A 0.01 Ry (0.14 eV) Gaussian broadening of electronic eigenvalues has been applied to simulate a DOS in order to clarify the spin up and spin down Co(3d) contributions to the molecular orbitals. Filled (non filled) curves indicate occupied (unoccupied) molecular orbitals. A light blue arrow indicates the minority highest single-occupied molecular orbital (SOMO) of all the systems.

Table III: **Calculated and measured oxidation potential vs SHE values.** Oxidation potential values vs SHE calculated and measured in the case of the CoCat models and of the Cu(I)/Cu(II), Fe(II)/Fe(III), Co(II)/Co(III) reference species

Species	$E^0$ (exp.) <sup>21,34</sup>	$E^0$ (DFT(PBE))	$E^0$ (DFT+U)
Cu(I)/Cu(II)	0.16	0.19	0.02
Fe(II)/Fe(III)	0.77	0.85	0.77
Co(II)/Co(III)	1.82	1.70	2.02
CoCat 0/+1	1.18	0.60	1.07
CoCat +1/+2	1.18	1.38	1.49
CoCat +2/+3	1.18	1.58	1.64
CoCat +3/+4	1.18	1.84	1.87

$\epsilon_{\text{VBM}}$ , i. e., the potential energy of the highest occupied electronic level, or the maximum of the valence band (VBM), of the host. The Fermi level defines the chemical potential of the electrons, assumed in a reservoir in contact with the system, and available in order to change the charge state of the dopant agent. In the present case, we have considered the CoCat models as dopant agents, and the water solution as host matrix. The calculation of formation energies permits to estimate transition energy levels,  $\epsilon^{q/q+1}$ , corresponding to the chemical potential of electrons at which the  $q$  and  $q + 1$  charge states of  $M$  have the same  $\Omega_f$ , that is, the Fermi level value at which the species  $M^q$  and  $M^{q+1}$  are in equilibrium. These transition levels are often found to be in a very good agreement with the available experimental measurements of the ionization energies of such defects. As mentioned above, an extension of Eq. (1) to molecules, considered as surface defects of a  $\text{TiO}_2$  host, is straightforward.<sup>32</sup> In the present study, we have further extended the investigation of transition energy levels to metal atoms and cluster, considered as dopant agents of an amorphous network of water molecules, representing the host matrix.

We have focused first on the oxidation potential of single metal ions; the  $\epsilon^{q/q+1}$  values of the Cu(I)/Cu(II), Fe(II)/Fe(III), and Co(II)/Co(III) couples have been calculated. In detail,  $M^q[\text{H}_2\text{O}]_6$  complexes have been surrounded with further 64 water molecules, distributed by using the PACK-MOL program,<sup>35</sup> in the same cubic supercell used in the AIMD simulations of the c1 cluster. The amount of molecules has been chosen and checked in order to minimize the stress tensor, i. e., the system pressure. All the systems have been then fully optimized. It may be noted that a first order

Makov-Payne correction<sup>36</sup> to the total energy of charged supercells is negligible, given the high dielectric constant of water (80, at 300 K), which provides an efficient screening of the charge of metal ions. The achieved  $\epsilon^{q/q+1}$  values are referred to the water O(2p) “valence band”, which is aligned to the zero energy value in the DOS plots of all the M(aq) systems, as shown in Figure S7. The potential energy values of the minority highest single-occupied molecular orbitals (SOMO) of the Cu(I), Fe(II), Co(II) hydrated ions, indicated by light blue arrow in Figure S7, provide a first indication of the difference between the oxidation potential of the three investigated ions. Such SOMO orbitals accommodate the electrons which are subtracted to the metal ions to form the oxidized hydrated Cu(II), Fe(III) and Co(III) species, and the expected potential energy order (Cu(I)>Fe(II)>Co(II)) is indeed found. The differences between  $\epsilon^{q/q+1}$  transition energy values, referenced to the O (2p) HOMO, and oxidation potentials, referenced to the standard hydrogen electrode (SHE), have been minimized in order to compare measured and calculated values. The achieved results are in good agreement with the measured values, in the case of both DFT(PBE) and DFT+U calculations, as reported in Table SIII. An Hubbard U correction of 5.9 eV, have been used in the case to the Cu, Fe and Co 3d shells, respectively, in order to be consistent with the total energy values with the ones obtained in the case of the CoCat model. It may be noted that an automatic alignment to the NHE potential could be achieved in the framework of a different ab initio method,<sup>37</sup> which, at variance with the present approach, can be applied to electrode semireactions involving proton coupled electron transfer processes only.

Reassured by the succesful extension of the method to the estimate of electrode potentials, we have calculated the potential at which electrons are exchanged between the solvated c1 cluster and the external circuit, as representative estimates of the working potential of the CoCat. This has been done by calculating the related  $\epsilon^{q/q+1}$  transition energy levels. Both DFT(PBE) and DFT+U results indicate that the first electron is subtracted to the cluster at a potential level which is lower than the external potential applied to the CoCat cell, as shown in the “CoCat 0/+1” row of Table SIII. This is in agreement with the fact that the removal of a single electron from the CoCat model does not favor the formation of an O-O bond, as detailed in the main text. The removal of

a second electron from the c1 cluster occurs at an estimated potential higher but still compatible with the working potential of the catalyst, and leads to an energetically favoured formation of the O-O bond. The removal of further electrons from the catalyst models raises the potential up to the values of the Co(II)/Co(III) couple. This quite high oxidation potential has been exploited in the molecular dynamics simulations to lower the potential energy barriers to the formation of the first Co=O intermediate of the evolution of an oxygen molecule, as discussed in the main text.

## References

- (1) Mattioli, G.; Risch, M.; Amore Bonapasta, A.; Dau, H.; Guidoni, L. *Phys. Chem. Chem. Phys.* **2011**, *13*, 15437.
- (2) Johnston, W. D.; Heikes, R. R.; Sestrich, D. *J. Phys. Chem. Solids* **1958**, *7*, 1.
- (3) Shao-Horn, Y.; Hackney, S. A.; Kahaian, A. J.; Thackeray, M. M. *J. Solid State Chem.* **2002**, *168*, 60.
- (4) Troullier, N.; Martins, J. L. *Phys. Rev. B* **1991**, *43*, 1993.
- (5) Heyd, J.; Scuseria, G. E.; Ernzerhof, M. *J. Chem. Phys.* **2003**, *118*, 8207–8215.
- (6) Heyd, J.; Scuseria, G. E.; Ernzerhof, M. *J. Chem. Phys.* **2006**, *124*, 219906.
- (7) Mattioli, G.; Alippi, P.; Filippone, F.; Caminiti, R.; Amore Bonapasta, A. *J. Phys. Chem. C* **2010**, *114*, 21694.
- (8) van Elp, J.; Wieland, J. L.; Eskes, H.; Kuiper, P.; Sawatzky, G. A.; de Groot, F. M. F.; Turner, T. S. *Phys. Rev. B* **1991**, *44*, 6090.
- (9) Galakhov, V. R.; Kurmaev, E. Z.; Uhlenbrock, S.; Neumann, M.; Kellerman, D. G.; Gorshkov, V. S. *Solid State Comm.* **1996**, *99*, 221.
- (10) Martyna, G. J.; Tuckerman, M. E. *J. Chem. Phys.* **1999**, *110*, 2810.

- (11) Cococcioni, M.; de Gironcoli, S. *Phys. Rev. B* **2005**, *71*, 035105.
- (12) Cohen, A. J.; Mori-Sánchez, P.; Yang, W. *Science* **2008**, *321*, 792–794.
- (13) Kulik, H. J.; Cococcioni, M.; Scherlis, D. A.; Marzari, N. *Phys. Rev. Lett.* **2006**, *97*, 103001.
- (14) Scherlis, D. A.; Cococcioni, M.; Sit, P.; Marzari, N. *J. Phys. Chem. B* **2007**, *111*, 7384–7391.
- (15) Mattioli, G.; Melis, C.; Malloci, G.; Filippone, F.; Alippi, P.; Giannozzi, P.; Mattoni, A.; Amore Bonapasta, A. *J. Phys. Chem. C* **2012**, *116*, 15439–15448.
- (16) Todorova, T.; Seitsonen, A. P.; Hutter, J.; Kuo, I.-F. W.; Mundy, C. J. *J. Phys. Chem. B* **2006**, *110*, 3685–3691.
- (17) Baroni, S.; de Gironcoli, S.; Dal Corso, A.; Giannozzi, P. *Rev. Mod. Phys.* **2001**, *73*, 515.
- (18) Eisenberg, D.; Kauzmann, W. *The structure and properties of water*; Oxford University Press, London, 1969.
- (19) Risch, M.; Khare, V.; Zaharieva, I.; Gerencser, L.; Chernev, P.; Dau, H. *J. Am. Chem. Soc.* **2009**, *131*, 6936.
- (20) Grimme, S. *J. Comput. Chem.* **2006**, *27*, 1787.
- (21) Surendranath, Y.; Kanan, M. W.; Nocera, D. G. *J. Am. Chem. Soc.* **2010**, *132*, 16501.
- (22) Lutterman, D. A.; Surendranath, Y.; Nocera, D. G. *J. Am. Chem. Soc.* **2009**, *131*, 3838.
- (23) Surendranath, Y.; Lutterman, D. A.; Liu, Y.; Nocera, D. G. *J. Am. Chem. Soc.* **2012**, *134*, 6326.
- (24) Risch, M.; Ringleb, F.; Khare, V.; Chernev, P.; Zaharieva, I.; Dau, H. *J. Phys.: Conf. Series* **2009**, *190*, 012167.
- (25) Wang, L.-P.; Van Voorhis, T. *J. Phys. Chem. Lett.* **2011**, *2*, 2200.

- (26) Baruah, T.; Pederson, M. R. *Chem. Phys. Lett.* **2002**, *360*, 144.
- (27) McAlpin, J. G.; Stich, T. A.; Ohlin, C. A.; Surendranath, Y.; Nocera, D. G.; Casey, W. H.; Britt, R. D. *J. Am. Chem. Soc.* **2011**, *133*, 15444.
- (28) Dismukes, G. C.; Brimblecombe, R.; Felton, G. A. N.; Pryadun, R. S.; Sheats, J. E.; Spiccia, L.; Swiegers, G. F. *Acc. Chem. Res.* **2009**, *42*, 1935.
- (29) Liu, X.; Wang, F. *Coord. Chem. Rev.* **2012**, *256*, 1115.
- (30) Cao, C.; Hill, S.; Cheng, H.-P. *Phys. Rev. Lett.* **2008**, *100*, 167206.
- (31) Van de Walle, C. G.; Neugebauer, J. *J. Appl. Phys.* **2004**, *95*, 3851–3879.
- (32) Mattioli, G.; Filippone, F.; Amore Bonapasta, A. *J. Am. Chem. Soc.* **2006**, *128*, 13772–13780.
- (33) Mattioli, G.; Filippone, F.; Caminiti, R.; Amore Bonapasta, A. *J. Phys. Chem. C* **2008**, *112*, 13579–13586.
- (34) Zoski, C. *Handbook of Electrochemistry*; Elsevier B. V., 2006.
- (35) Martinez, L.; Andrade, R.; Birgin, E. G.; Martinez, J. M. *J. Comp. Chem.* **2009**, *30*, 2157–2164.
- (36) Makov, G.; Payne, M. C. *Phys. Rev. B* **1995**, *51*, 4014.
- (37) Norskov, J. K.; Rossmeisl, J.; Logadottir, A.; Lindqvist, L.; Kitchin, J. R.; Bligaard, T.; Jonsson, H. *J. Phys. Chem. B* **2004**, *108*, 17886–17892.